A Supramolecular Approach for Liver Radioembolization

Spa, S.J.; Welling, M.M.; Oosterom, M.N. van; Rietbergen, D.D.D.; Burgmans, M.C.; Verboom, W.; ... ; Leeuwen, F.W.B. van

IVYSPRING INTERNATIONAL PUBLISHER

Theranostics

2018; 8(9): 2377-2386. doi: 10.7150/thno.23567

Research Paper

A Supramolecular Approach for Liver Radioembolization

Silvia J. Spa,[1,2*] Mick M. Welling,[1*] Matthias N. van Oosterom,[1] Daphne D. D. Rietbergen,[1,3] Mark C. Burgmans,[4] Willem Verboom,[5] Jurriaan Huskens,[5] Tessa Buckle,[1] and Fijs W. B. van Leeuwen [1, 2]✉

1. Interventional Molecular Imaging Laboratory, Department of Radiology, Leiden University Medical Center, Leiden, The Netherlands.
2. Department of Agrotechnology and Food services, subdivision BioNanoTechnology, Wageningen University, Wageningen, The Netherlands
3. Department of Radiology, Nuclear Medicine Section, Leiden University Medical Center, Leiden The Netherlands.
4. Interventional Radiology, Department of Radiology, Leiden University Medical Center, Leiden, The Netherlands
5. Molecular NanoFabrication group, MESA+ Institute for Nanotechnology, University of Twente, Enschede, The Netherlands

*These authors contributed equally to this work

✉ Corresponding author: F.W.B. van Leeuwen, email: F.W.B.van_Leeuwen@lumc.nl, tel: +31-(0)715266029

Received: 2017.10.30; Accepted: 2018.01.18; Published: 2018.03.23

Abstract

Hepatic radioembolization therapies can suffer from discrepancies between diagnostic planning (scout-scan) and the therapeutic delivery itself, resulting in unwanted side-effects such as pulmonary shunting. We reasoned that a nanotechnology-based pre-targeting strategy could help overcome this shortcoming by directly linking pre-interventional diagnostics to the local delivery of therapy.

Methods: The host-guest interaction between adamantane and cyclodextrin was employed in an *in vivo* pre-targeting set-up. Adamantane (guest)-functionalized macro albumin aggregates (MAA-Ad; d = 18 μm) and (radiolabeled) Cy5 and β-cyclodextrin (host)-containing PIBMA polymers (^{99m}Tc-Cy5$_{0.5}$CD$_{10}$PIBMA$_{39}$; MW ~ 18.8 kDa) functioned as the reactive pair. Following liver or lung embolization with (^{99m}Tc)-MAA-Ad or (^{99m}Tc)-MAA (control), the utility of the pre-targeting concept was evaluated after intravenous administration of ^{99m}Tc-Cy5$_{0.5}$CD$_{10}$PIBMA$_{39}$.

Results: Interactions between MAA-Ad and Cy5$_{0.5}$CD$_{10}$PIBMA$_{39}$ could be monitored in solution using confocal microscopy and were quantified by radioisotope-based binding experiments. *In vivo* the accumulation of the MAA-Ad particles in the liver or lungs yielded an approximate ten-fold increase in accumulation of ^{99m}Tc-Cy5$_{0.5}$CD$_{10}$PIBMA$_{39}$ in these organs (16.2 %ID/g and 10.5 %ID/g, respectively) compared to the control. Pre-targeting with MAA alone was shown to be only half as efficient. Uniquely, for the first time, this data demonstrates that the formation of supramolecular interactions between cyclodextrin and adamantane can be used to drive complex formation in the chemically challenging *in vivo* environment.

Conclusion: The *in vivo* distribution pattern of the cyclodextrin host could be guided by the pre-administration of the adamantane guest, thereby creating a direct link between the scout-scan (MAA-Ad) and delivery of therapy.

Key words: Nanotechnology, Interventional radiology, Pre-targeting, Supramolecular chemistry, Radioembolization

Introduction

Radioembolization is a radiation-based therapeutic method that is applied for primary liver tumors and metastases that are untreatable via surgery or chemotherapy. During these interventions, microspheres that contain therapeutic radioisotopes (β-emitters such as yttrium-90 or holmium-166) are intrahepatically delivered.[1] While the clinical benefit of this approach has been demonstrated in large

randomized controlled trials,[2-4] the preclusion of hepatopulmonary shunting remains an unsolved challenge. Shunting results in the displacement of a fraction of the administered particles towards the microvasculature of the lung instead of the liver, leading to ineffective dose distribution and serious adverse effects such as radiation pneumonitis.[5-7] To predict the likelihood of shunting prior to initiation of the therapeutic intervention, technetium-99m labeled macro albumin aggregates (^{99m}Tc-MAA; d = 18 μm) can be administered as a diagnostic "scout" procedure. Besides insight into the degree of shunting, SPECT/CT-based ^{99m}Tc-MAA uptake monitoring also helps to provide a dosimetric (distribution) model for the therapeutic isotopes.[6,8] Differences in particle composition and pharmacokinetics, however, do not fully exclude discrepancies between the "scout" procedure and the therapeutic delivery. As a result, hepatopulmonary shunting still occurs in over 13% of therapeutic interventions.[9-11] Unfortunately, when this occurs the implementation of preventive measures is no longer an option.

In an attempt to provide a more advanced theranostic solution for this problem, we investigated a two-step pre-targeting concept *in vivo*. The potential of an *in vivo* pre-targeting setup has been shown in radioimmunotherapy of cancer which has relied on, for example, the interactions between complementary oligonucleotides,[12] or bispecific- or avidin/biotin-antibodies.[13] However, this setup suffered from slow pharmacokinetics (at least 2 d between the first two injections), possible internalization of the antibody, and/or requires multiple (3-5) injection steps.[13] To overcome these issues a different pre-targeting approach based on multivalent supramolecular host-guest interactions between adamantane (Ad) and β-cyclodextrin (CD; Figure 1A) was investigated. While CD has been utilized to form nanoparticles for drug delivery [14,15] the host-guest chemistry was always performed beforehand, and not in situ. Recently, we successfully employed CD-Ad host-guest chemistry *in vitro* [16,17] and, to the best of our knowledge, we now employ these chemical CD-Ad host-guest interactions *in vivo* for the first time.

Using Ad_x-guest-functionalized MAA microspheres (Figure 1A), the diagnostic MAA compound was converted into a pre-targeting vector for an intravenously (i.v.) administered radiolabeled β-cyclodextrin-PIBMA-polymer (host, Figure 1A). The β-cyclodextrin-polymer provides a platform for future functionalization with therapeutic radioisotopes. The pre-targeted radioembolization concept was tested via the use of two different pre-clinical models that were either in line with: 1) the routine clinical use of ^{99m}Tc-MAA for lung staining, wherein MAA is administered intravenously (i.v.; Model I, Figure 1B), or 2) the current clinical set-up for locally administered hepatic radioembolization wherein MAA is administered locally (Model II, Figure 1C).

Experimental

General

For the stability of the compounds please see the Supplementary Material section. All chemicals were obtained from commercial sources and used without further purification. NMR spectra were obtained using a Bruker DPX 300 spectrometer (300 MHz, ^{1}H NMR) or a Bruker AVANCE III 500 MHz with a TXI gradient probe. All spectra were referenced to residual solvent signal or TMS. HPLC was performed on a Waters system using a 1525EF pump and a 2489 UV detector. For preparative HPLC, a Dr. Maisch GmbH, Reprosil-Pur 120 C18-AQ 10 μm column and a gradient of 0.1 % TFA in H_2O/CH_3CN (95:5) to 0.1 % TFA in H_2O/CH_3CN (5:95) in 40 min were used. For analytical HPLC, a Dr. Maisch GmbH, Reprosil-Pur C18-AQ 5 μm (250×4.6 mm) column and a gradient of 0.1 % TFA in H_2O/CH_3CN (95:5) to 0.1 % TFA in H_2O/CH_3CN (5:95) in 40 min were used. MALDI-ToF measurements were performed on a Bruker Microflex. High-resolution mass spectra were measured on an Exactive orbitrap high-resolution mass spectrometer (Thermo Fisher Scientific, San Jose, CA) and processed with the use of Thermo Scientific Xcalibur software (V2.1.0.1139). For dialysis, Sigma Pur-A-Lyzer™ Mega 3,500 units were used.

Synthesis

Adamantane-tetrafluorophenol (Ad-TFP)

1-Adamantanecarboxylic acid (500 mg, 2.8 mmol) and 2,3,5,6-tetrafluorophenol (TFP) (718 mg, 4.3 mmol) were dissolved in 10 mL dry dichloromethane (DCM) and stirred for 10 min. Subsequently, *N,N*-dicyclohexylcarbodiimide (858 mg, 4.3 mmol), dissolved in 5 mL dry DCM, was added drop-wise. After stirring for 2 days at RT, the reaction mixture was filtered and the filtrate was concentrated in vacuo. The resulting yellow product was purified by silica column chromatography (DCM:Hexane, 1:1). Pure fractions were pulled and concentrated under vacuum to obtain the product as a white crystalline powder (785 mg, 86%). ^{1}H NMR (300 MHz, $CDCl_3$, 25 ^{o}C) = δ 7.06 – 6.89 (m, 1H, CH of TFP), 2.09 (s, 9H, C-$\underline{CH_2}$-CH and CH_2-$\underline{CH}$-CH_2), 1.78 (s, 6H, CH-$\underline{CH_2}$-CH). High resolution mass: $[C_{17}H_{17}F_4O_2]^+$ calculated 329.3, found 328.1 (Figure S1).

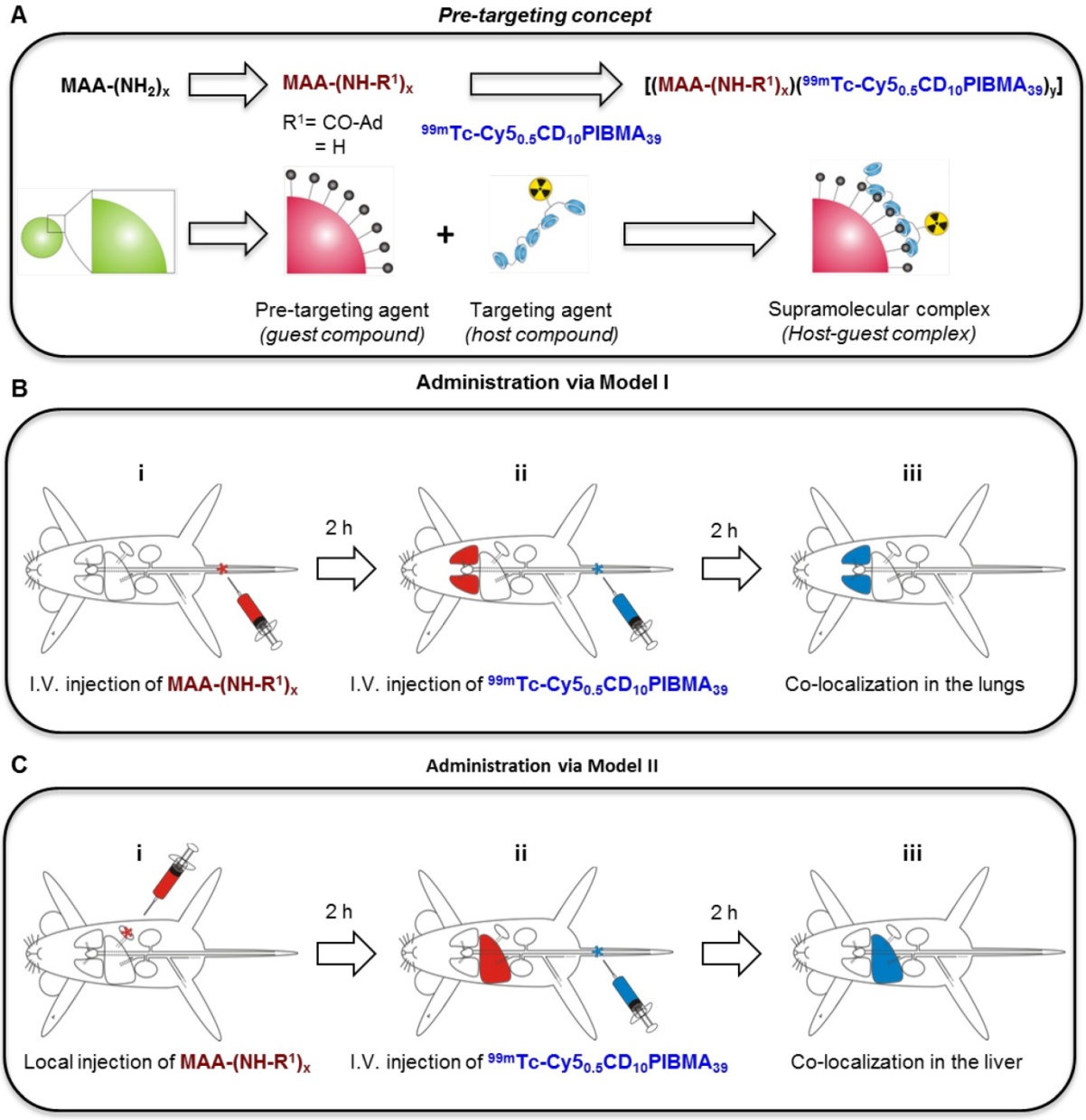

Figure 1. Schematic illustration of the radioembolization tailored pre-targeting concept including the chemical and functional steps involved. A) Representation of the different chemical functionalities and components. B) I.v. pre-administered MAA-Ad (Bi) accumulated in the lungs (Bii). Subsequent i.v. administration of ^{99m}Tc-Cy5$_{0.5}$CD$_{10}$PIBMA$_{39}$ (Bii) resulted in pulmonary co-localization of MAA-Ad and ^{99m}Tc-Cy5$_{0.5}$CD$_{10}$PIBMA$_{39}$ (Biii). C) Locally pre-administered MAA-Ad (Ci) accumulated in the liver (Cii). Following i.v. administration of ^{99m}Tc-Cy5$_{0.5}$CD$_{10}$PIBMA$_{39}$ (Cii), hepatic co-localization of both compounds was observed (Ciii).

Cy5-(SO$_3$)Sulfonate-(SO$_3$)COTFP

Cy5-(SO$_3$)Sulfonate-(SO$_3$)COOH was synthesized according to a previously published procedure.[18]

Cy5$_{0.5}$CD$_{10}$PIBMA$_{39}$

The synthesis of Cy5$_{0.5}$CD$_{10}$PIBMA$_{39}$ was performed according to a recently described procedure.[16]

Functionalization of macro-aggregates with adamantane (MAA-Ad)

Albumin macro-aggregates (TechneScan®, MAA) were obtained from Mallinckrodt Medical B.V., Petten, The Netherlands. Lyophilized macro-aggregates (2 mg) were dissolved in 1 mL of saline (0.9% NaCl, sterile and pyrogen-free, B. Braun Medical Supplies, Inc., Oss, The Netherlands) and portions of 0.1 mL (containing 0.2 mg MAA) were stored in Eppendorf tubes at -20 °C until further use. For functionalization, one portion was defrosted and 20 µL of Ad-TFP (10 mg/mL DMSO) was added. After agitation in a shaking water bath for 1 h at 37 °C, the solution was washed 2 times with phosphate buffered saline (PBS) by 2 centrifugation steps (3 min, 3000 ×g). The obtained MAA-Ad was diluted in 1 mL of PBS to 0.2 mg/mL.

To estimate the number of Ad conjugated to MAA, the MAA functionalization was also performed with Cy5-TFP according to the same procedure as for Ad-TFP. Subsequently, the absorbance at 650 nM of the MAA-Cy5 constructs was measured using a NanoDrop Spectrophotometer (Thermo Fisher Scientific Inc. Wilmington, DE, USA). The dye concentration was calculated using the absorbance following the law of Lambert Beer ($A = \varepsilon \cdot l \cdot C$) with $\varepsilon_{Cy5} = 250 \times 10^3$ $mol^{-1}cm^{-1}$. The number of Cy5/MAA aggregates was then calculated by dividing the calculated Cy5 concentration by the known MAA concentration, resulting in a ratio of $3.07(\pm0.24)x10^8$ Cy5/MAA particle on average. Assuming that Ad-TFP reacts in a similar fashion as Cy5-TFP, it was estimated that the ratio of Ad/MAA would be of the same order of magnitude.

Radiolabeling of $Cy5_{0.5}CD_{10}PIBMA_{39}$

To 10 µL of $Cy5_{0.5}CD_{10}PIBMA_{39}$ (1 mg/mL in PBS), 4 µL of $SnCl_2.2H_2O$ (0.44 mg/mL saline, Technescan PYP, Mallinckrodt Medical B.V.), and 100 µL of a freshly eluted ^{99m}Tc-Na-pertechnetate solution (500 MBq/mL, Mallinckrodt Medical B.V.) were added and the mixture was gently stirred in a shaking water bath for 1 h at 37 °C.[19] Subsequently, the labeling yield was estimated over time by ITLC analysis. Here fore 2 µL of the reaction mixture was applied on 1x7 cm ITLC-SG paper strips (Agilent Technologies, USA) for 10 min at RT with PBS as the mobile phase. After 1 h, the highest labeling yield of $Cy5_{0.5}CD_{10}PIBMA_{39}$ with ^{99m}Tc was assessed (49.6%) and the reaction mixture was purified by size exclusion chromatography with sterile PBS as the mobile phase using Sephadex™ G-25 (desalting columns PD-10, GE Healthcare Europe GmbH, Freiburg, Germany). Fractions containing ^{99m}Tc-$Cy5_{0.5}CD_{10}PIBMA_{39}$ were collected and directly applied in the imaging experiments.

Radiostability in PBS

To assess the stability of the radiolabeling in PBS, the release of radioactivity from PD-10-purified ^{99m}Tc-$Cy5_{0.5}CD_{10}PIBMA_{39}$ was determined with ITLC at 24 h (according to the same method described in 'Radiolabeling of $Cy5_{0.5}CD_{10}PIBMA_{39}$').

Supramolecular interaction between MAA-Ad and ^{99m}Tc-$Cy5_{0.5}CD_{10}PIBMA_{39}$

To determine the supramolecular interaction between MAA-Ad and $Cy5_{0.5}CD_{10}PIBMA_{39}$ *in vitro*, 0.1 mL of MAA-Ad in PBS (0.2 mg/mL) and 0.1 mL of ^{99m}Tc-$Cy5_{0.5}CD_{10}PIBMA_{39}$ in PBS (1 mg/mL, 1 MBq) were mixed and the solution was incubated for 1 h in a shaking water bath at 37 °C. Hereafter, the radioactivity of the total amount added and the radioactivity of the pellet after two washing steps with PBS were measured in a dose-calibrator to determine the amount of binding of ^{99m}Tc-$Cy5_{0.5}CD_{10}PIBMA_{39}$ to MAA-Ad. After correction for background activity, the amount of binding was expressed as the percentage of the total amount of radioactivity (%binding). To assess the effect of the Ad moieties, the same experiment was also performed with non-functionalized MAA and the resulting %binding of ^{99m}Tc-$Cy5_{0.5}CD_{10}PIBMA_{39}$ to MAA and MAA-Ad were compared (Figure 2B). Significance between the two conditions was calculated using a two-tailed student's t-Test with n = 4.

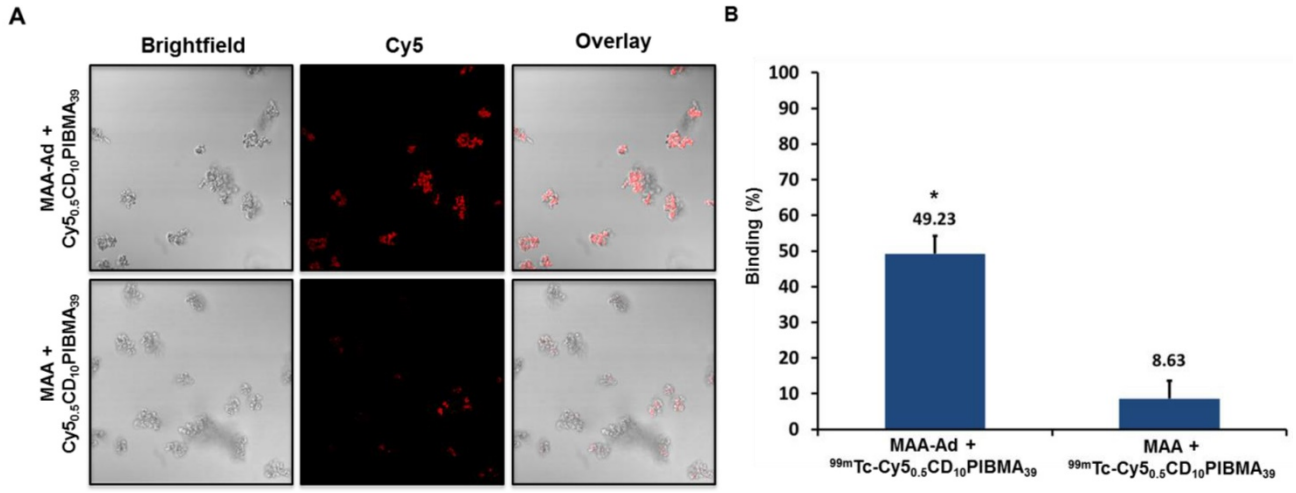

Figure 2. A) Fluorescence confocal microscopy-based evaluation of $Cy5_{0.5}CD_{10}PIBMA_{39}$ (Cy5) binding to MAA-Ad (top) and non-functionalized MAA (bottom). The MAA-Ad-localized particles (brightfield) revealed a higher degree of staining compared to MAA alone, indicated by the higher Cy5-related fluorescence intensities (in red). B) The binding of ^{99m}Tc-$Cy5_{0.5}CD_{10}PIBMA_{39}$ to MAA-Ad and MAA quantified by radioactivity and expressed as a percentage of the total amount of radioactivity (^{99m}Tc-$Cy5_{0.5}CD_{10}PIBMA_{39}$) added. Compared to non-functionalized MAA, binding of ^{99m}Tc-$Cy5_{0.5}CD_{10}PIBMA_{39}$ to MAA functionalized with the Ad guest moiety was 5.7 times higher ($P < 0.01$).

The supramolecular interaction between MAA-Ad and $Cy5_{0.5}CD_{10}PIBMA_{39}$ was also visualized by confocal microscopy using the Cy5 component of the polymer.[16] For this purpose, non-radioactive $Cy5_{0.5}CD_{10}PIBMA_{39}$ was added to the MAA and MAA-Ad solutions. After washing, 10 µL of MAA (with or without-Ad) $Cy5_{0.5}CD_{10}PIBMA_{39}$ solution was pipetted onto culture dishes with glass inserts (ø35mm glass bottom dishes No. 15, poly-d-lysine coated, γ-irradiated, MatTek corporation). Images were acquired using a Leica SP5 WLL confocal microscope (λ_{ex} 633 nm, λ_{em} 650-700 nm) under 63x magnification using Leica Application Suite software.

In vivo studies

Animals

All *in vivo* studies were performed using 10-12 week old Swiss mice (20-25 g, Crl:OF1 strain, Charles River Laboratories, USA). All animal studies were approved by the institutional Animal Ethics Committee (DEC permit 12160) of the Leiden University Medical Center. All mice were kept under specific pathogen-free conditions in the animal housing facility of the LUMC. Food and water were given *ad libitum*.

General SPECT imaging and biodistribution protocol

SPECT imaging was performed at 2 h after injection of ^{99m}Tc-labeled compounds. Mice were placed onto a dedicated positioning bed of a three-headed U-SPECT-2 (MILabs, Utrecht, the Netherlands) under continuous 1-2% isoflurane anesthesia.[20] Radioactivity counts from total body scans or selected regions of interest (ROI) were acquired for 60 min using a 0.6 mm mouse multi-pinhole collimator in list mode data. For reconstruction from list mode data, the photo peak energy window was centered at 140 keV with a window width of 20%. Side windows of 5% were applied to correct for scatter and down scatter corrections. The image was reconstructed using 24 Pixel based Ordered Subset Expectation Maximization iterations (POSEM) with 4 subsets, 0.2 mm isotropic voxel size and with decay and triple energy scatter correction integrated into the reconstruction with a post filter setting of 0.25 mm.[21] Volume-rendered images were generated from 2-4 mm slices and analyzed using Matlab R2014a software (version 8.3.0.532, MathWorks® Natick, MA). Images were generated from maximum intensity protocols (MIP) adjusting the color scale threshold to optimal depiction of the tissues of interest.[22] After imaging, the mice were euthanized by an intraperitoneal injection of 0.25 mL Euthasol (ASTfarma, Oudewater, The Netherlands).

To determine the biodistribution of the tracer, organs were collected and counted for radioactivity in a dose-calibrator (VDC 101, Veenstra Instruments, Joure, the Netherlands) or a gamma counter (Wizard2 2470 automatic gamma scintillation counter, Perkin Elmer). After excision of the tissues and determination of the activity remaining in the carcass, the total amount of remaining radioactivity in the animal was counted and the urinary excretion expressed as the percentage of the total injected dose (%ID) was calculated (corrected for decay). Radioactive counts in tissues were expressed as the percentage of the total injected dose of radioactivity per gram tissue (%ID/g). Additionally, reconstructed images were generated and analyzed using Amide 1.0.2 software (http://amide.sourceforge.net/documentation.html).[23]

Mapping the distribution of ^{99m}Tc-$Cy5_{0.5}CD_{10}PIBMA_{39}$ in mice

To determine the natural distribution of ^{99m}Tc-$Cy5_{0.5}CD_{10}PIBMA_{39}$, 0.1 mL of PBS containing ^{99m}Tc-$Cy5_{0.5}CD_{10}PIBMA_{39}$ (1 mg/mL, 20 MBq) was injected i.v. 2 h after injection, SPECT imaging and biodistribution studies were performed as described above (Figure 3A, D).

Mapping the distribution of ^{99m}Tc-labeled MAA-Ad in mice via:

i.v. administration, Model I

To determine whether MAA-based embolization is tolerated by mice, and whether MAA-Ad is delivered to the capillaries of the lungs, MAA-Ad was radiolabeled according to the manufacturer's instructions. Hereafter 0.1 mL of ^{99m}Tc-MAA-Ad in PBS (0.02 mg, 2 mg/mL) was injected into the tail vein. At 2 h after injection, the organ distribution of the tracer in mice was imaged using SPECT and quantified with biodistribution studies (see SPECT imaging protocol and biodistribution studies described above; Figure 3 B, D).

Local administration, model II

An embolization setup in the liver was performed to mimic the clinical setup for liver radioembolization.[24] For this purpose, animals were anesthetized by intraperitoneal injection of a mixture containing Hypnorm (Vetapharma, Leeds, United Kingdom), dormicum (Roche, Basel, Switzerland), and water (1:1:2). After shaving and cleaning with ethanol (70%), the abdominal cavity was incised for 0.5 cm and the spleen was exposed. Of the ^{99m}Tc-MAA-Ad solution (2 mg/mL), 100 µL was injected into the spleen using a Myjector U-100 insulin syringe (29G x ½" 0.33 x12 mm, Terumo Europe, Leuven, Belgium) and after 5 s the needle was removed and

the spleen was repositioned in the peritoneal cavity. The incision was sutured by 2-4 stitches and the animals were placed under a heating lamp to maintain the body temperature at 37 °C. At 2 h after injection, the organ distribution of the tracer in mice was imaged using SPECT and quantitated with biodistribution studies as described above (Figure 3C, D).

Mapping the distribution of ^{99m}Tc-Cy5$_{0.5}$CD$_{10}$PIBMA$_{39}$ after MAA(-Ad) pre-administration

The influence of MAA or MAA-Ad on the distribution of ^{99m}Tc-Cy5$_{0.5}$CD$_{10}$PIBMA$_{39}$ was evaluated using 0.1 mL containing MAA-Ad or non-functionalized MAA in 0.1 mL (0.02 mg, 2 mg/mL), injected either via i.v. (Figure 1B, Model I) or local administration (Figure 1C, Model II). At 2 h post MAA administration, 0.1 mL of ^{99m}Tc-Cy5$_{0.5}$CD$_{10}$PIBMA$_{39}$ in PBS (1 mg/mL, 20 MBq) was injected i.v. SPECT imaging and biodistribution studies were performed as described above at 2h after the second injection (Figure 4).

Results and Discussion

To allow for initial diagnostics of the particle distribution and to provide a guest-particle that can act as an *in vivo* target, clinical grade MAA particles were functionalized with Ad guest moieties (Figure 1A) via amide bond formation. This yielded MAA-Ad with, on average, 10^8 Ad molecules per MAA particle. Especially for these experiments a fluorescent β-cyclodextrin-poly(isobutylene-*alt*-maleic-anhydride)-polymer host molecule (Cy5$_{0.5}$CD$_{10}$PIBMA$_{39}$, ~18.8 kDa, diameter, ~11.7 nm) was synthesized (Figure 1A),[16] that contained (on average) ten β-CD compounds. Besides CD, various carboxylic acid groups were present on the backbone of the polymer that could serve as the chelating ligand for a range of metal ion-based radio-isotopes, such as ^{90}Y, ^{166}Ho, and ^{99m}Tc.

The interaction between CD and Ad is well-known, with a binding affinity of ~5×10^4 M^{-1} for a monovalent interaction.[25] Increasing the number of host and guest moieties drives multivalent interactions, which effectively increases the binding affinity.[26] Evidence that individual compounds effectively form complexes based on intended Ad-CD binding interactions was demonstrated *in vitro*. While MAA alone did induce some Cy5$_{0.5}$CD$_{10}$PIBMA$_{39}$ accumulation, clearly a higher level of Cy5$_{0.5}$CD$_{10}$PIBMA$_{39}$ accumulation was obtained with MAA-Ad (Figure 2A). The difference in accumulation was quantified by a radioisotope-based binding experiment with ^{99m}Tc-Cy5$_{0.5}$CD$_{10}$PIBMA$_{39}$. This experiment revealed a significant ($p < 0.01$) 5.7-fold increase (Figure 2B) in ^{99m}Tc-Cy5$_{0.5}$CD$_{10}$PIBMA$_{39}$ accumulation with MAA-Ad (49.2%) versus MAA (8.6%), underlining that the observed complex formation is indeed facilitated by the intended Ad-CD host-guest interactions.

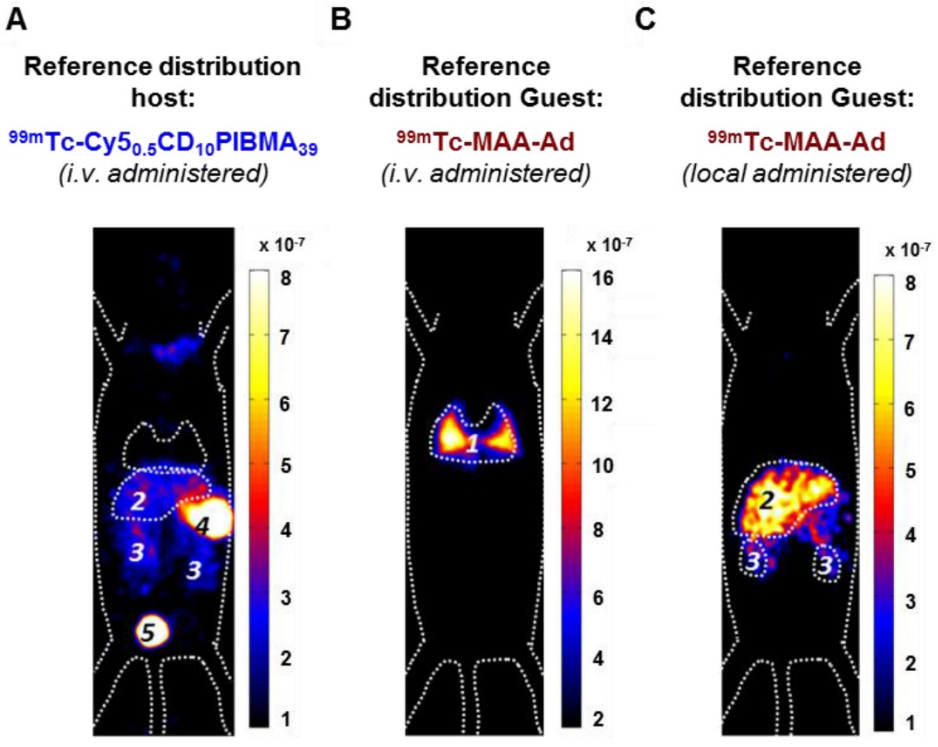

Figure 3. Reference SPECT and biodistribution data of A) i.v.-administered ^{99m}Tc-Cy5$_{0.5}$CD$_{10}$PIBMA$_{39}$, and B) i.v.- or C) locally administered ^{99m}Tc-MAA-Ad. Organs are marked as (1) lungs, (2) liver, (3) kidneys, (4) stomach, and (5) urinary bladder.

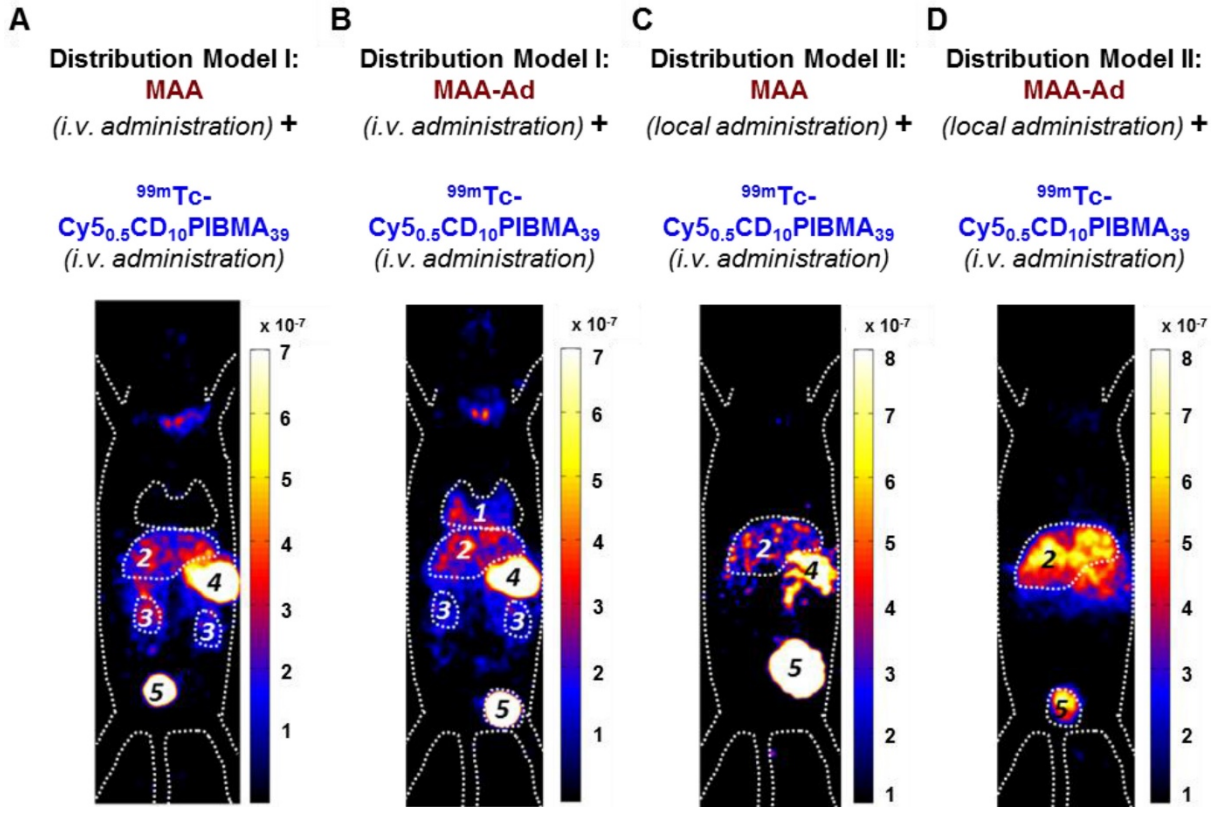

Figure 4. SPECT and biodistribution data of i.v.-administered ^{99m}Tc-Cy5$_{0.5}$CD$_{10}$PIBMA$_{39}$ after pre-targeting with MAA or MAA-Ad either i.v.- (Model I) or locally (Model II) administered. A) Following i.v. administration of MAA, no pulmonary accumulation of ^{99m}Tc-Cy5$_{0.5}$CD$_{10}$PIBMA$_{39}$ was observed. B) i.v. pre-administered Ad-functionalized MAA did lead to pulmonary accumulation of ^{99m}Tc-Cy5$_{0.5}$CD$_{10}$PIBMA$_{39}$. C) Following local administration of MAA, slight uptake in liver and kidneys occurred. D) After pre-targeting with MAA-Ad, the hepatic accumulation of ^{99m}Tc-Cy5$_{0.5}$CD$_{10}$PIBMA$_{39}$ was even more profound. Organs are marked as (1) lungs, (2) liver, (3) kidneys, (4) stomach, and (5) urinary bladder.

To create a reference for the *in vivo* binding between Cy5$_{0.5}$CD$_{10}$PIBMA$_{39}$ and MAA-Ad, first the biodistribution of i.v. administered ^{99m}Tc-Cy5$_{0.5}$CD$_{10}$PIBMA$_{39}$ was studied without any pre-targeting vector present. This yielded a low overall organ uptake (~1.5 %ID/g, Figure 3A, D). Secondly, the distribution of the pre-targeting vector ^{99m}Tc-MAA-Ad in both the i.v. and local administration model was determined. SPECT imaging and biodistribution studies at 2 h post tracer administration revealed a distinct distribution pattern of ^{99m}Tc-MAA-Ad for Model I (i.v.) and Model II (local, Figure 3A, 3B). In agreement with previous reports on the distribution of ^{99m}Tc-MAA after i.v. injection,[27] Model I showed high levels of accumulation of ^{99m}Tc-MAA-Ad in the lungs (335 %ID/g). Local administration of ^{99m}Tc-MAA-Ad, whereby hepatic tracer delivery was realized through injection into parenchymal tissue of the spleen (Model II),[28] resulted in high uptake levels in the liver (50.4 %ID/g).

The influence of local MAA(-Ad) deposits on the distribution of i.v.-administered ^{99m}Tc-Cy5$_{0.5}$CD$_{10}$PIBMA$_{39}$ was studied via Model I (Figure 1B). Here the biodistribution of ^{99m}Tc-Cy5$_{0.5}$CD$_{10}$PIBMA$_{39}$ after i.v. pre-administration of MAA and MAA-Ad (Figure 4A, B) was compared with the reference distribution of ^{99m}Tc-Cy5$_{0.5}$CD$_{10}$PIBMA$_{39}$ (no MAA-(Ad) administered, Figure 3A, S2). Pre-targeting with non-functionalized MAA did not lead to changes in the distribution of ^{99m}Tc-Cy5$_{0.5}$CD$_{10}$PIBMA$_{39}$ (Figure 4A, S2). More specifically, uptake levels in both the lungs and liver remained around 1.5 %ID/g (Figure 4E, 5A). Pre-targeting with MAA-Ad, however, did induce clear alterations in the distribution pattern of ^{99m}Tc-Cy5$_{0.5}$CD$_{10}$PIBMA$_{39}$ (Figure 4B) as uptake in the lungs increased 6.2-fold (10.5 %ID/g, Figure 4E, 5A). Interestingly, the uptake in the liver also increased towards 5.7 %ID/g, while both the i.v. administration of ^{99m}Tc-MAA-Ad and ^{99m}Tc-Cy5$_{0.5}$CD$_{10}$PIBMA$_{39}$ alone did not lead to significant liver uptake. It appears that the presence of ^{99m}Tc-Cy5$_{0.5}$CD$_{10}$PIBMA$_{39}$ influenced the retention of MAA-Ad, causing partial displacement of the (complexed) compounds towards the liver. Alternatively, Ad-labeled metabolites of MAA-Ad could have migrated to the liver, thereby providing a platform for ^{99m}Tc-Cy5$_{0.5}$CD$_{10}$PIBMA$_{39}$ binding.

To assess the value of pre-targeting in the liver, which is representative of the clinical radioembolization procedure, the same host-guest setup was

applied following intrahepatic deposition (Model II; Figure 1C). In this model, the influence of MAA-Ad was even more profound. The presence of low quantities of uptake in the salivary glands and the stomach (Table S1, Figure S2) is indicative for the presence of some free ^{99m}Tc[29] (see Supplementary Material for further stability details). Compared to the control, pre-targeting with non-functionalized MAA resulted in increased uptake levels of ^{99m}Tc-$Cy5_{0.5}CD_{10}PIBMA_{39}$ in the liver (8.7 %ID/g) and kidneys (10.7 %ID/g), but not in the lungs (1.4 %ID/g, Table 1 vs. Figure 4C, Table 2). This complex formation is in line with that observed during the radioisotope-based *in vitro* binding experiments in solution (Figure 2). After pre-targeting with MAA-Ad, the differences became more distinct, yielding a 15.7-fold increase in liver uptake (16.2 %ID/g) and a 4.5-fold increase in kidney uptake (19.6 %ID/g) (Figure 4D, E, 5B). Both uptake profiles are in accordance with the distribution pattern of locally administered ^{99m}Tc-MAA-Ad (Figure 3C). As was concluded from the in situ binding, the liver uptake induced by MAA-Ad was nearly double that observed using MAA only. Clearly the host-guest complex formation is more efficient in the liver than in the lungs (see Figure 5). This is likely to be related to the 1,000-fold reduction in particle velocity experienced as they traverse the vasculature of the liver, a feature that was said to result in 7.5-times higher interaction rates between particles and hepatic cells.[30] The flow reduction may also be enhanced further following partial blockage (embolization) of capillary vessels by MAA(-Ad).

Table 1. Biodistribution of i.v.-administered ^{99m}Tc-$Cy5_{0.5}CD_{10}PIBMA_{39}$ and i.v.- or locally administered ^{99m}Tc-MAA-Ad.

	Reference distribution host	Reference distribution guest	
Tissue	^{99m}TC-$Cy5_{0.5}CD_{10}PIBMA$ mean	Model I: ^{99m}Tc-MAA-Ad mean	Model II: ^{99m}Tc-MAA-Ad mean
Blood	2.4 ± 1.3	2.7 ± 0.9	1.0 ± 0.6
Lungs	1.7 ± 0.5	335.8 ± 38.7	4.4 ± 1.2
Spleen	0.9 ± 0.4	0.9 ± 0.2	6.1 ± 2.4
Liver	1.0 ± 0.2	1.3 ± 0.4	50.4 ± 15.4
Kidneys	4.7 ± 1.3	1.8 ± 0.6	15.3 ± 2.7
Muscle	0.4 ± 0.2	0.3 ± 0.1	0.9 ± 0.3
Brain	0.1 ± 0.0	0.1 ± 0.1	0.2 ± 0.1

Data were calculated based on the radioactive counts measured in various tissues at 2 h post-injection of the radioactive tracer expressed as the mean of the percentage of the injected dose per gram tissue (%ID/g) of 5 observations.

Taken together, the combined distribution data for Model I and Model II clearly indicate that the *in vivo* distribution pattern of the multimeric ^{99m}Tc-$Cy5_{0.5}CD_{10}PIBMA_{39}$ host molecule, which served as a model for a future therapeutic agent, can be guided by a pre-targeting approach that makes use of Ad-functionalized microspheres. The fact that the supramolecular interactions in the liver are stronger than those in the lungs indicates that in this pre-targeting model, pulmonary shunting during liver embolization procedures would only result in limited unwanted side-effects. Furthermore, although not yet explored in this study, in the future the polymer-based building blocks can be synthetically modified to: i) optimize their pharmacokinetics and ii) act as carriers for other (therapeutic) isotopes or drugs, e.g., for chemo-embolization.[29,31,32] Alternatively, local (e.g. intratumoral) deposits of albumin-based particles could not only be used to mark tumors for surgical resection.[33] In a pre-targeting approach such particles could also help provide local therapy.

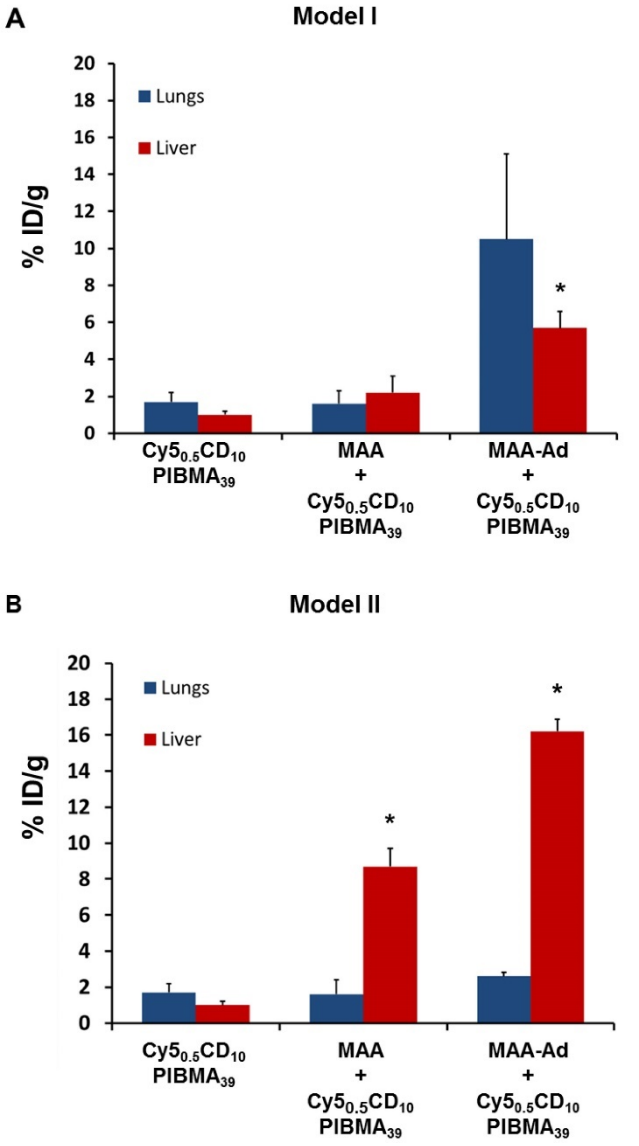

Figure 5. Influence of MAA(-Ad) on the uptake of ^{99m}Tc-$Cy5_{0.5}CD_{10}PIBMA_{39}$ in the lungs and liver (Table 1 and 2). A) Uptake in the lungs increased when MAA-Ad was administered i.v. (Method I). B) Increasing uptake in the liver was seen when MAA-Ad was administered locally (Method II). The significance of difference ($P < 0.01$) is indicated with *.

In previous studies we have demonstrated that supramolecular chemistry can be used to generate clinical grade imaging agents, such as indocyanine green (ICG)-^{99m}Tc-nanocolloid.[31,32] This multimodal nanoparticle has helped to connect pre- and intra-operative imaging, and as such, realized imaging-guided surgery of infected lymph nodes. In the present study, we successfully applied a different supramolecular interaction *in vivo* to advance a theranostic medical intervention, namely radioembolization.

Table 2. Biodistribution of ^{99m}Tc-Cy5$_{0.5}$CD$_{10}$PIBMA$_{39}$ after pre-targeting with i.v.- (Model I) or locally (Model II) administered MAA or MAA-Ad.

	Distribution of host (^{99m}Tc-Cy5$_{0.5}$CD$_{10}$PIBMA$_{39}$) following injection of indicated guest			
	Model I: MAA	**Model I: MAA-Ad**	**Model II: MAA**	**Model II: MAA-Ad**
Tissue	Mean	Mean	Mean	mean
Blood	2.1 ± 1.0	1.9 ± 0.5	1.9 ± 0.3	3.8 ± 0.6
Lungs	1.6 ± 0.7	10.5 ± 4.6	1.4 ± 07	2.6 ± 0.2
Spleen	1.2 ± 0.4	4.7 ± 2.3	4.7 ± 1.3	10.4 ± 1.4
Liver	2.2 ± 0.9	5.7 ± 0.9	8.7 ± 1.0	16.2 ± 0.7
Kidneys	4.1 ± 1.7	6.6 ± 2.0	10.7 ± 0.8	19.6 ± 3.8
Muscle	0.5 ± 0.2	0.5 ± 0.2	0.5 ± 0.1	0.8 ± 0.4
Brain	0.3 ± 0.4	0.2 ± 0.2	0.1 ± 0.1	0.1 ± 0.0

Data were calculated based on the radioactive counts measured in various tissues at 2 h post-injection of the radioactive tracer expressed as the mean of the percentage of the injected dose per gram tissue (%ID/g) of 5 observations.

Conclusion

The initial proof-of-concept data presented demonstrates that despite the chemically complex *in vivo* environment, multivalent host-guest interactions between Ad and CD can still be formed. Depending on the route of MAA-Ad administration (i.v. or local), the degree and location of ^{99m}Tc-Cy5$_{0.5}$CD$_{10}$PIBMA$_{39}$ accumulation could be guided. For future radio-embolization applications this would mean that the distributions observed in the scout scan would directly correlate to those of the therapeutic radioisotope delivery (e.g., ^{90}Y or ^{166}Ho). Overall, a versatile new chemical platform for translational theranostic pre-targeting has been generated.

Abbreviations

Ad: adamantane; CD: β-cyclodextrin; CT: computed tomography; DCM: dichloromethane; i.v.: intravenously; MAA: macro albumin aggregates; PIBMA: poly (isobutylene – *alt* – maleic - anhydride); SPECT: single photon emission computed tomogramphy; TFP: tetrafluorophenyl.

Acknowledgements

The research leading to these results was funded with grants from: the European Research Council (ERC) under the European Union's Seventh Framework Program FP7/2007-2013 (grant agreement number 2012-306890), from the Netherlands Organization for Scientific Research (NWO nano-Grant STW 11435 and VIDI-grant - STW BGT11272) and the 2015-2016 Postdoctoral Molecular Imaging Scholar Program Grant granted by the Society of Nuclear Medicine and Molecular Imaging (SNMMI) and the Education and Research Foundation (ERF) for Nuclear Medicine and Molecular Imaging. We acknowledge Mark T. M. Rood for providing Cy5$_{0.5}$CD$_{10}$PIBMA$_{39}$.

Supplementary Material

Supplementary figures and tables.
http://www.thno.org/v08p2377s1.pdf

Competing Interests

The authors have declared that no competing interest exists.

References

1 Hickey R, Lewandowski RJ, Prudhomme T, et al. 90Y Radioembolization of Colorectal Hepatic Metastases Using Glass Microspheres: Safety and Survival Outcomes from a 531-Patient Multicenter Study. J Nucl Med. 2016; 57: 665-71.
2 Hilgard P, Hamami M, Fouly AE, et al. Radioembolization with yttrium-90 glass microspheres in hepatocellular carcinoma: European experience on safety and long-term survival. Hepatology. 2010; 52: 1741-9.
3 Kennedy A, Coldwell D, Sangro B, et al. Radioembolization for the treatment of liver tumors general principles. Am J Clin Oncol. 2012; 35: 91-9.
4 Rosenbaum CE, Verkooijen HM, Lam MG, et al. Radioembolization for treatment of salvage patients with colorectal cancer liver metastases: a systematic review. J Nucl Med. 2013; 54: 1890-5.
5 Cremonesi M, Chiesa C, Strigari L, et al. Radioembolization of hepatic lesions from a radiobiology and dosimetric perspective. Front Oncol. 2014; 4: 210.
6 Braat AJAT, Smits MLJ, Braat MNGJA, et al. 90Y Hepatic Radioembolization: An Update on Current Practice and Recent Developments. J. Nucl. Med. 2015; 56: 1079-87.
7 van den Hoven AF, Rosenbaum CE, Elias SG, et al. Insights into the Dose-Response Relationship of Radioembolization with Resin 90Y-Microspheres: A Prospective Cohort Study in Patients with Colorectal Cancer Liver Metastases. J Nucl Med. 2016; 57: 1014-9.
8 Shanehsazzadeh S, Lahooti A, Yousefnia H, et al. Comparison of estimated human dose of (68)Ga-MAA with (99m)Tc-MAA based on rat data. Ann Nucl Med. 2015; 29: 745-53.
9 Garin E, Rolland Y, Laffont S, et al. Clinical impact of (99m)Tc-MAA SPECT/CT-based dosimetry in the radioembolization of liver malignancies with (90)Y-loaded microspheres. Eur J Nucl Med Mol Imaging. 2016; 43: 559-75.
10 Leung TW, Lau WY, Ho SK, et al. Radiation pneumonitis after selective internal radiation treatment with intraarterial 90yttrium-microspheres for inoperable hepatic tumors. Int. J. Radiat. Oncol. Biol. Phys. 1995; 33: 919-24.
11 Jha AK, Purandare N, Shah SA, et al. Is there a correlation between planar scintigraphy after Tc-99m-MAA and Y-90 administration? Nucl. Med. Commun. 2016; 37: 107-09.
12 Patra M, Zarschler K, Pietzsch HJ, et al. New insights into the pretargeting approach to image and treat tumours. Chem Soc Rev. 2016; 45: 6415-31.
13 Boerman OC, van Schaijk FG, Oyen WJG, et al. Pretargeted Radioimmunotherapy of Cancer: Progress Step by Step. J Nucl Med. 2003; 44: 400-11.
14 Gaur S, Wang Y, Kretzner L, et al. Pharmacodynamic and pharmacogenomic study of the nanoparticle conjugate of camptothecin CRLX101 for the treatment of cancer. Nanomedicine. 2014; 10: 1477-86.
15 Dan Z, Cao H, He X, et al. Biological stimuli-responsive cyclodextrin-based host-guest nanosystems for cancer therapy. Int J Pharm. 2015; 483: 63-8.
16 Rood MT, Spa SJ, Welling MM, et al. Obtaining control of cell surface functionalizations via Pre-targeting and Supramolecular host guest interactions. Sci Rep. 2017; 7: 39908.
17 Oikonomou M, Wang J, Carvalho RR, et al. Ternary supramolecular quantum-dot network flocculation for selective lectin detection. Nano Res. 2016; 9: 1904-12.

18 Spa SJ, Bunschoten A, Rood MTM, et al. Orthogonal Functionalization of Ferritin via Supramolecular Re-Assembly. Eur J Inorg Chem. 2015; 2015: 4603-10.
19 Welling MM, Paulusma-Annema A, Balter HS, et al. Technetium-99m labelled antimicrobial peptides discriminate between bacterial infections and sterile inflammations. Eur J Nucl Med. 2000; 27: 292-301.
20 Welling MM, Bunschoten A, Kuil J, et al. Development of a Hybrid Tracer for SPECT and Optical Imaging of Bacterial Infections. Bioconjugate Chem. 2015; 26: 839-49.
21 Branderhorst W, Vastenhouw B & Beekman FJ. Pixel-based subsets for rapid multi-pinhole SPECT reconstruction. Phys. Med. Biol. 2010; 55: 2023-34.
22 van Oosterom MN, Kreuger R, Buckle T, et al. U-SPECT-BioFluo: an integrated radionuclide, bioluminescence, and fluorescence imaging platform. EJNMMI Res. 2014; 4: 56-56.
23 Loening AM & Gambhir SS. AMIDE: a free software tool for multimodality medical image analysis. Mol. Imaging. 2003; 2: 131-7.
24 Kasuya H, Kuruppu DK, Donahue JM, et al. Mouse models of subcutaneous spleen reservoir for multiple portal venous injections to treat liver malignancies. Cancer. Res. 2005; 65: 3823-7.
25 Eftink MR, Andy ML, Bystrom K, et al. Cyclodextrin Inclusion Complexes: Studies of the Variation in the Size of Alicyclic Guests. Journal of the American Chemical Society. 1989; 111: 6765-72.
26 Mulder A, Auletta T, Sartori A, et al. Divalent binding of a Bis(adamantyl)-functionalized calix[4]arene to cyclodextrin-based hosts: An Experimental and Theoretical Study on Multivalent Binding in Solution and at Self-Assembled Monolayers. Journal of the American Chemical Society. 2004; 126: 6627-36.
27 Chandra R, Shamoun J, Braunstein P, et al. Clinical Evaluation of an Instant Kit for Preparation of 99mTc-MAA for Lung Scanning. J Nucl Med. 1973; 14: 702-05.
28 Kasuya H, Kuruppu DK, Donahue JM, et al. Mouse Models of Subcutaneous Spleen Reservoir for Multiple Portal Venous Injections to Treat Liver Malignancies. Cancer Res. 2005; 65: 3823-27.
29 Irwin RS, Doherty PW, Bartter T, et al. Evaluation of Technetium Pertechnetate as a Radionuclide Marker of Pulmonary Aspiration of Gastric Contents in Rabbits. Chest. 1988; 93: 1270-75.
30 Tsoi KM, MacParland SA, Ma XZ, et al. Mechanism of hard-nanomaterial clearance by the liver. Nat Mater. 2016; 15: 1212-21.
31 Brouwer OR, van den Berg NS, Matheron HM, et al. A hybrid radioactive and fluorescent tracer for sentinel node biopsy in penile carcinoma as a potential replacement for blue dye. Eur Urol. 2014; 65: 600-9.
32 van den Berg NS, Brouwer OR, Schaafsma BE, et al. Multimodal Surgical Guidance during Sentinel Node Biopsy for Melanoma: Combined Gamma Tracing and Fluorescence Imaging of the Sentinel Node through Use of the Hybrid Tracer Indocyanine Green–99mTc-Nanocolloid. Radiology. 2015; 275: 521-29.
33 KleinJan GH, Brouwer OR, Matheron HM, et al. Hybrid radioguided occult lesion localization (hybrid ROLL) of (18)F-FDG-avid lesions using the hybrid tracer indocyanine green-(99m)Tc-nanocolloid. Rev Esp Med Nucl Imagen Mol. 2016; 35: 292-7.